

# Novel Metal-Based Luminophores for Biological Imaging

David Lloyd, Michael P. Coogan, and Simon J.A. Pope

**Abstract** This review aims to summarise key recent developments regarding the use of luminescent metal complexes in biological imaging. The photophysical advantages of *d*- and *f*-block complexes are discussed and specific examples of cellular imaging are described through confocal fluorescence microscopy studies. Issues of complex design and specific organelle targeting are considered together with the use of a phosphorescent ruthenium complex to monitor intracellular oxygen levels in real-time, via microscopy and time-resolved luminescence methods. The development of near-IR-emissive probes based on lanthanide complexes are also briefly presented, together with strategies for their application as responsive reporters in a biological context.

## 1 Introduction

The use of biological imaging is central to the elucidation of key questions in the continuing search for molecular mechanisms that underpin biomedical, veterinary, agricultural and industrial problems. Such problems often necessitate novel probes with exploitable luminescent properties. Luminescent metal coordination complexes are increasingly seen as attractive candidates for such tasks due to their dual applicability to (a) optical imaging and (b) targeted molecular probes. Those based

---

D. Lloyd (✉)

Department of Microbiology, Cardiff Schools of Bioscience, Cardiff University, Main Building,  
Museum Avenue, Cathays Park, Cardiff CF10 3AT, Wales, UK  
e-mail: lloyd@cardiff.ac.uk

M.P. Coogan • S.J.A. Pope

Cardiff School of Chemistry, Cardiff University, Main Building, Museum Avenue,  
Cathays Park, Cardiff CF10 3AT, Wales, UK

upon either platinum-group or lanthanide-series metal ions have many desirable and wide-ranging properties for such applications. These can include:

- Tunable emission throughout the visible and near-IR regions
- Long luminescence lifetimes (from hundreds of nanosecond to millisecond domain)
- Good luminescence quantum yields, sometimes exceeding 0.5
- Large Stokes shifts (often  $>5,000\text{ cm}^{-1}$ )
- Good thermal, chemical and photochemical stability and metabolic inertness [1–9]

Biological criteria for the ideal luminescent probe include: (a) rapid penetration of the compound into the cell; (b) uniform distribution within the highly structured and compartmentalised cellular ultrastructure; (c) well-defined characteristics of alterations in absorption and emission (absorption coefficients and quantum yields) that may result from binding to cellular molecular constituents or membranes; (d) the presence of probe should be without metabolic effects and (e) for long-term monitoring, they should not influence either survival or the capacity for cellular growth and reproduction.

The application of late-transition metal complexes, and especially polypyridyl complexes, in biological imaging has been the focus of a great deal of interest with  $d^6$ -transition metal complexes, such as  $\text{Re}^{\text{I}}$  [2–4],  $\text{Ru}^{\text{II}}$  [5] and  $\text{Ir}^{\text{III}}$  [6] in particular, showing useful application in cellular imaging studies. The emissive lanthanide ions also offer additional opportunities for luminophore design and application. For example, complexes of  $\text{Eu}(\text{III})$ ,  $\text{Tb}(\text{III})$  and  $\text{Sm}(\text{III})$  offer visible luminescence [10], whereas  $\text{Nd}(\text{III})$ ,  $\text{Er}(\text{III})$  and  $\text{Yb}(\text{III})$  possess low-energy emission extending well into the near-IR region [11]. In all cases, the nature of the lanthanide-based emission differs fundamentally from those  $d$ -metal complexes discussed above, originating from  $4f$ -(metal) centred excited states. Relaxation from these excited states is formally forbidden, resulting therefore in very long emission lifetimes that typically range from millisecond (Eu and Tb) through microseconds ( $\text{Yb}(\text{III})$ ) to nanoseconds ( $\text{Nd}(\text{III})$ ) domains. Cellular imaging with visibly emissive  $\text{Ln}(\text{III})$  complexes is now established utilising both macrocyclic [7] and helical bimetallic complexes [8], but further development towards deeper tissue imaging requires the use of low-energy wavelengths (i.e. near IR) since biological tissue possesses a much greater transparency to near-IR wavelengths in comparison to visible and UV wavelengths. In this regard,  $\text{Ln}(\text{III})$  complexes again have much to offer since  $\text{Nd}(\text{III})$ ,  $\text{Pr}(\text{III})$ ,  $\text{Er}(\text{III})$  and  $\text{Yb}(\text{III})$  are all emissive in the near-IR region, and as the technology of sensitive, near-IR detection improves complexes based on these ions may be extremely useful in optical imaging applications involving confocal fluorescence and lifetime imaging microscopy.

## 2 Development and Application of Novel $d^6$ -Transition Metal Luminophores

Luminescent  $d^6$  complexes of  $\text{Ir}(\text{III})$  [12],  $\text{Re}(\text{I})$  [13] and  $\text{Ru}(\text{II})$  [14] with polypyridyl or organometallic ligands are attractive for application in imaging due to common characteristics, including the kinetic inertness of low spin  $d^6$  octahedral

complexes, which is important to prevent ligand substitution and associated toxicity and for air and water stability; large Stokes shifts ( $>100$  nm); long luminescence lifetimes (hundreds of ns to  $\mu$ s) and high photostability (low photobleaching). In order to overcome problems associated with membrane permeability and uptake, some groups have chosen to conjugate such complexes to biomolecules [4, 5] or incorporate lipophilic entities into their complexes [6]. Ir and Ru are promising candidates for these applications, but Re has particular features, which make it an attractive candidate, in that the excited state is localised on a single ligand, allowing a degree of tuning in the emission characteristics, and the axial (usually, a pyridine) ligand therefore allows a photophysically innocent point for attachment of, e.g. lipophilic groups to assist the uptake.

## 2.1 Rhenium Complexes in Sensing Applications

Rhenium complexes have been applied as chemosensors or probes for molecules and ions and, in particular, cationic rhenium complexes have been proposed as anion sensors [15]. Rhenium  $^3$ MLCT emission can also be sensitive to the presence of dissolved dioxygen and rhenium complexes have also been shown to be capable of indicating oxygen levels by luminescence lifetime [16], although none have been applied in cellular oxygen mapping. DeGraff and Demas [17] used the protection of the excited state of rhenium complexes in macromolecules to show responses to cyclodextrins through host–guest interactions.

A rhenium complex functionalised with an alkyl chain has been developed as a probe for the local environment through a hydrophobically driven chain-wrapping mechanism inducing lengthening of the excited state lifetime in water. However, in the presence of proteins containing a fatty acid-binding pocket or lipid membranes, the alkyl chain is extended leaving the excited state exposed to solvent, resulting in a shorter lifetime [3, 18].

In a rare example of cation sensing, encapsulation of a silver ion in a neutral luminescent rhenium macrocyclic ligand changes the system's emissivity giving a prototype metal-ion sensor [19]. Responsive, luminescent lifetime probes based upon axially functionalised fac-[Re(CO) $_3$ (di-imine)(L)] $^+$  complexes have also been prepared, where axial ligand, L, incorporates a binding site targeted towards metal cations of physiological and toxicological importance (Cu $^{2+}$ , Zn $^{2+}$  and Hg $^{2+}$ ). Cation binding in acetonitrile results in modulation of emission profiles and  $^3$ MLCT lifetimes and the latter parameter can be exploited to discriminate between analytes in an ionic background [20].

## 2.2 Rhenium Complexes in Cell Imaging Applications

The first report of a rhenium complex in fluorescent cell imaging [21] was of bisquinoline complexes conjugated to fMLF, a peptide previously used [22] in radioimaging

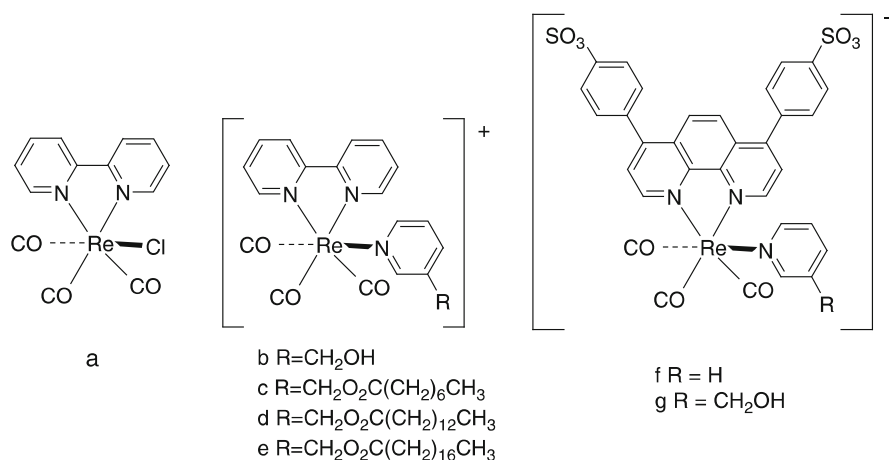


**Fig. 1** Rhenium complexes 1a–g applied in imaging in *Spironucleus vortens*

of formyl peptide receptor (FPR). By comparison with known FPR-targeting agents, it appeared that conjugation to the rhenium complex had not perturbed the localisation. This bisquinoline system has also been conjugated to cobalamin (B<sub>12</sub>) and shown, in cell imaging experiments, to target the cubilin receptor through the vitamin B12 uptake pathway [23]. Although this latter study used visible light excitation, most quinoline-based systems require UV excitation and thus polypyridines have dominated most recent rhenium imaging studies. In 2007, the first imaging applications of simple Re<sup>I</sup> species derived from polypyridines, such as bipy and phen, were reported [2, 24].

This report detailed the application of a range of cationic and anionic, polar and lipophilic rhenium complexes, all derived from the rhenium *fac*-tricarbonyl core. The polypyridine fragment was represented by phen, bipy and batho-phenanthroline sulphonate, with the axial ligand represented as chloride, pyridine, 3-hydroxymethylpyridine and aliphatic esters of 3-hydroxymethylpyridine (Fig. 1). A series of imaging experiments were undertaken in *Spironucleus vortens*, a parasitic flagellate chosen as prolific feeders which would allow investigation of Re<sup>I</sup> species in vivo.

This study demonstrated that while the basic core rhenium complex is non-toxic or of low toxicity over the timescale of the experiment, the ligands have a significant control of the toxicity of the complexes. The labile chloride ligand was shown to give a complex of high toxicity (as judged by *S. vortens*' motility). Presumably, loss of chloride anion gives a coordinatively unsaturated species which allows interaction with biomolecules, e.g. DNA bases. Less expectedly, the C<sub>18</sub> substituted complex also showed high toxicity at normal concentrations, apparently acting as a surfactant and leading to cell lysis (Fig. 2); however, at much lower concentrations, good uptake and low toxicity were observed.

The C<sub>12</sub> and C<sub>8</sub> analogues were also taken up well (Fig. 3), and showed low toxicity. Photobleaching, which can be a significant problem with conventional luminophores, was observed only with the chloride complex (at least under the

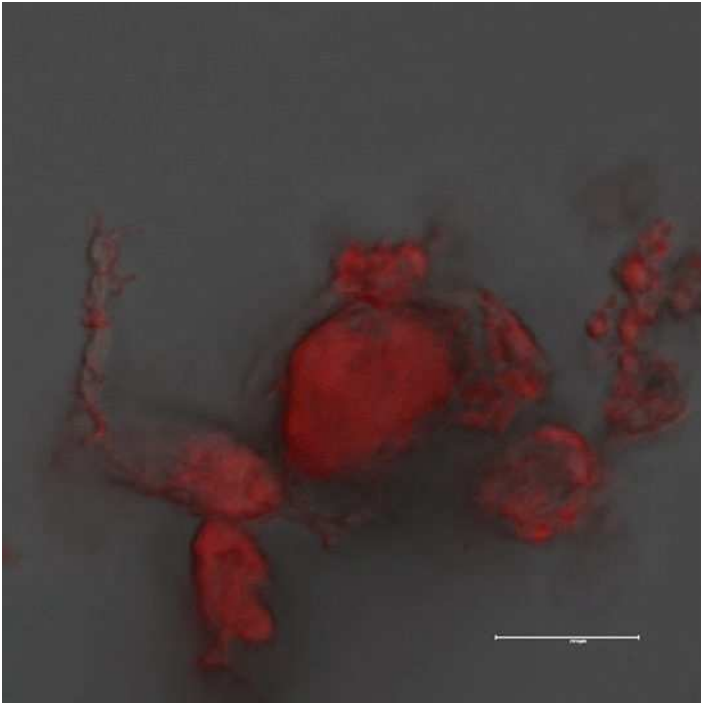


**Fig. 2** Cell lysis caused by **1e** in *Spironucleus vortens*. Scalebar=7.7  $\mu$ m

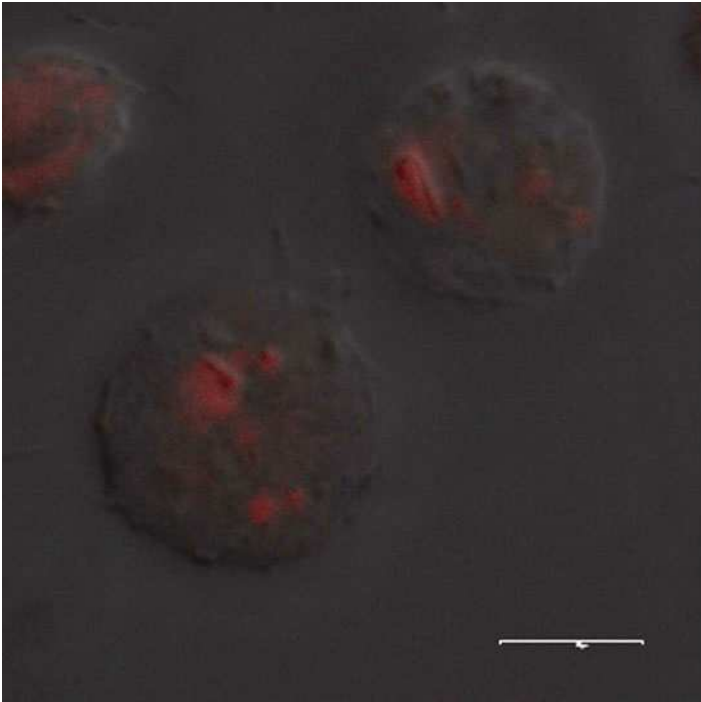


**Fig. 3** **1e** in *Spironucleus vortens*. Scalebar=5.5  $\mu$ m

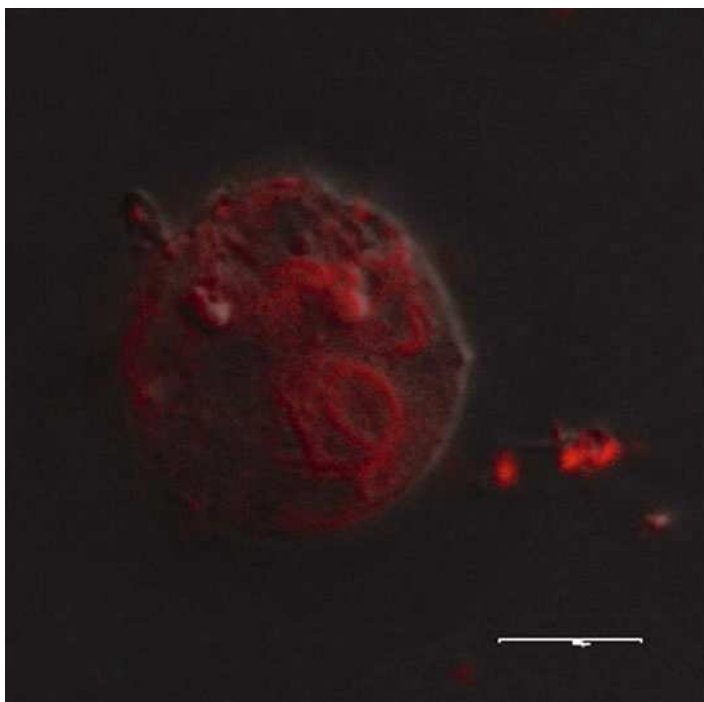
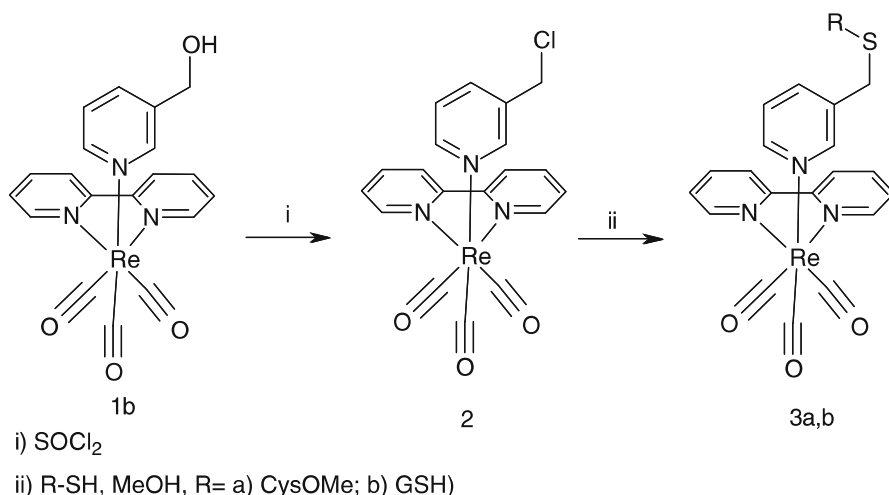


**Fig. 4** **1g** localising in vacuoles in *Spironucleus vortens*. Scalebar=6.0  $\mu\text{m}$

experimental conditions). This enhanced photostability of the less-reactive complexes is highly encouraging, and the reduced photostability of the labile chloride can be attributed to photolytic halide loss. Highly polar anionic complexes of the bathophenanthroline sulphonate ligand appeared to be localised in digestive vacuoles (Fig. 4), presumably uptake being by a phagocytotic mechanism.

The cationic complexes, which were assumed to be taken up by passive diffusion, distributed well throughout the membrane and membrane structures in the cytoplasm, indicating good permeability. The fine detail of ligand structure seems to have a significant effect on cytotoxicity, with unsubstituted pyridine complexes being more toxic than their 3-hydroxymethyl analogues.

Following this demonstration of the potential for rhenium complexes to be applied as imaging agents in fluorescence microscopy, the development of rhenium complexes, which could target specific organelles, was considered. While localisation in, e.g. vacuoles had been observed as a function of polarity and low membrane permeability, a more subtle and controlled targeting was desired. Cationic, thiol reactive species accumulate in mitochondria due to the potential gradient drawing cations into mitochondria and the high concentrations of reduced thiols found in mitochondria fixing the species by alkylation. The targeting of healthy mitochondria is an important goal in biological imaging and this potential and thiol-reactive



**Scheme 1** Synthesis of chloromethyl species and subsequent reactivity with thiol derivatives.

**Table 1** Electronic spectroscopy of thiol-reactive and thiolated complexes

Complex	$^1\text{IL}$ ( $\lambda_{\text{abs}}/\text{nm}$ )	$^1\text{MLCT}$ ( $\lambda_{\text{abs}}/\text{nm}$ )
2 <sup>a</sup>	248, 268 and 314	358
3a <sup>b</sup>	247 and 319	352
3b <sup>b</sup>	246, 269, 309 and 320	356

<sup>a</sup> $\text{CH}_3\text{CN}$  as solvent

<sup>b</sup> $\text{MeOH}$  as solvent

**Table 2** Emission and excitation spectra of thiol-reactive and thiolated complexes

Complex	Excitation ( $\lambda/\text{nm}$ )	Emission ( $\lambda/\text{nm}$ )	Lifetimes ( $\tau/\text{ns}$ )
2 <sup>a</sup>	364	551	131
3a <sup>b</sup>	360	550	122
3b <sup>b</sup>	361	551	116

<sup>a</sup> $\text{CH}_3\text{CN}$  as solvent

<sup>b</sup> $\text{MeOH}$  as solvent

targeting is the basis of the commercially available Mitotracker Red (chloromethyl-X-rosamine) [25].

Rhenium complexes with neutral ligands are intrinsically cationic and the *S. vortens*' work had shown them to be membrane permeable. While  $d^6$  luminophores with thiol-reactive groups have been known for over a decade [26, 27] prior to this study, none had been applied in imaging. A rhenium complex which localises in mitochondria would offer photophysical advantages, in terms of Stokes shift and lifetime, over conventional agents.

A thiol-reactive, cationic rhenium complex based around the rhenium *fac*-tricarbonyl core with a bipyridine unit to ensure useful luminescence and a chloromethyl-substituted

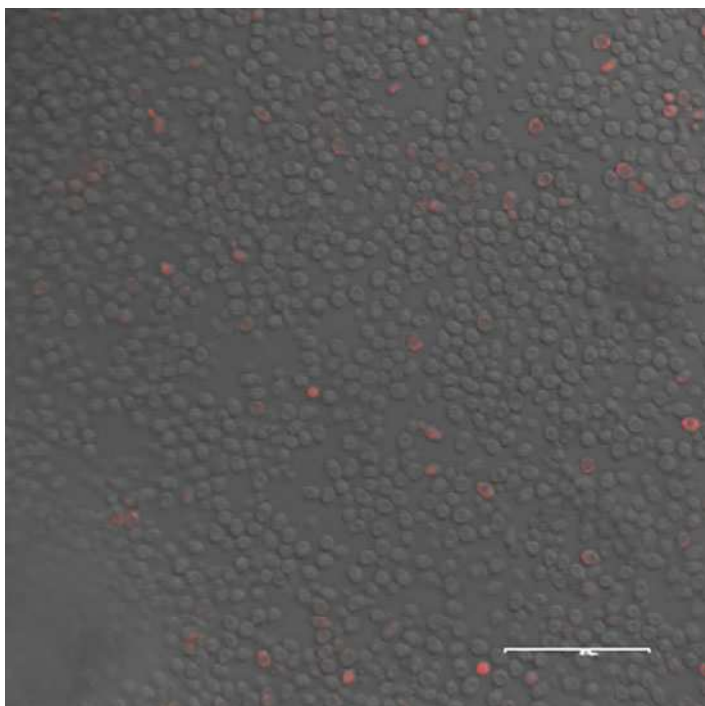


**Fig. 5** Chloromethyl complex **2** in yeast showing low level of uptake. Scale bar=47.6  $\mu\text{m}$

pyridine to endow thiol reactivity, was synthesised according to the route illustrated in Scheme 1.

This species showed the high reactivity towards thiols which had been hoped for, and both the agent and the products of reaction with bio-relevant thiols were also shown to retain the typical photophysical properties of  $\text{Re}^{\text{I}}$  bipy complexes in physiologically relevant media ( $\lambda_{\text{max ex}} \sim 360 \text{ nm}$ ,  $\lambda_{\text{max em}} \sim 550 \text{ nm}$ ,  $\tau \sim 100 \text{ ns}$ , broad excitation with significant absorption  $>400 \text{ nm}$ ) (Table 1).

The photophysical properties of thiol-reactive and thiolated complexes are summarised in Tables 1 and 2.

In an attempt to demonstrate that the chloromethyl complex **2** was a useful mitochondrial agent, it was incubated with yeast (*Saccharomyces cerevisiae*) as this is a well-characterised organism, which could assist in identifying patterns of localisation. In general, while certain cells in the sample showed good uptake, these represented only a small proportion of the population (Fig. 5). While those cells which had taken up the fluorophore appeared to show distinctive patterns of localisation (Fig. 6), the proportion was so small that this could not be taken as a demonstration of a useful mitochondrial-targeting agent. There appeared to be some preference for **2** to have localised in budding cells (Fig. 7).



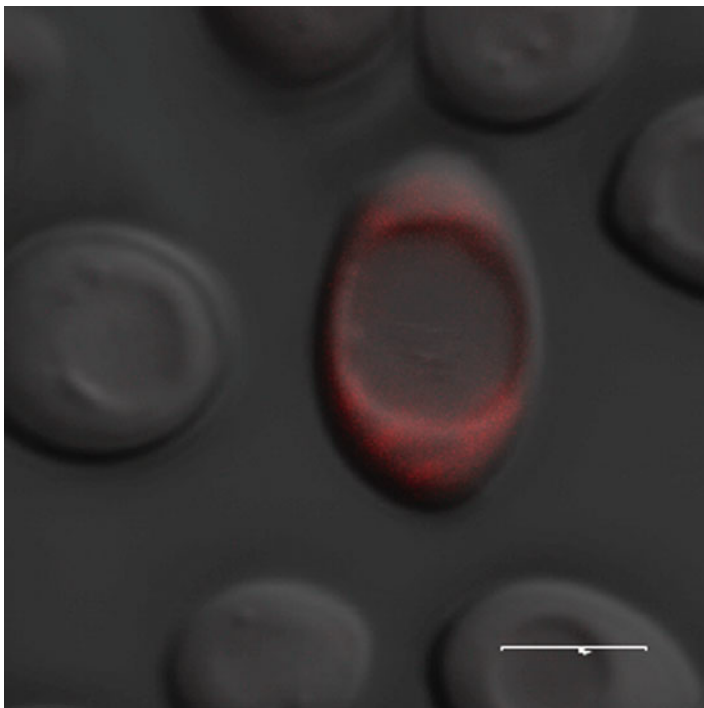


**Fig. 6** Chloromethyl complex **2** in yeast showing localisation. Scale bar=3.0 µm

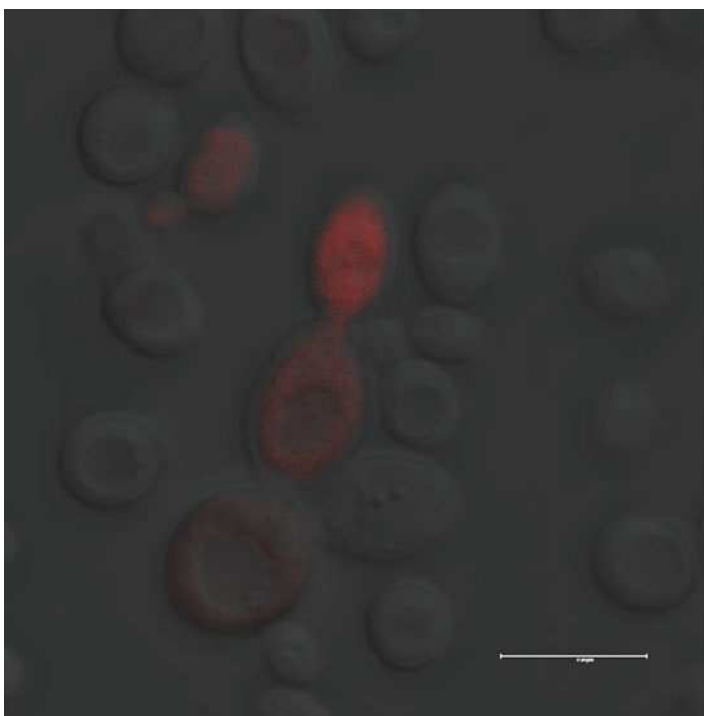


**Fig. 7** Chloromethyl complex **2** in yeast showing uptake in dividing cells. Scale bar=7.4 µm

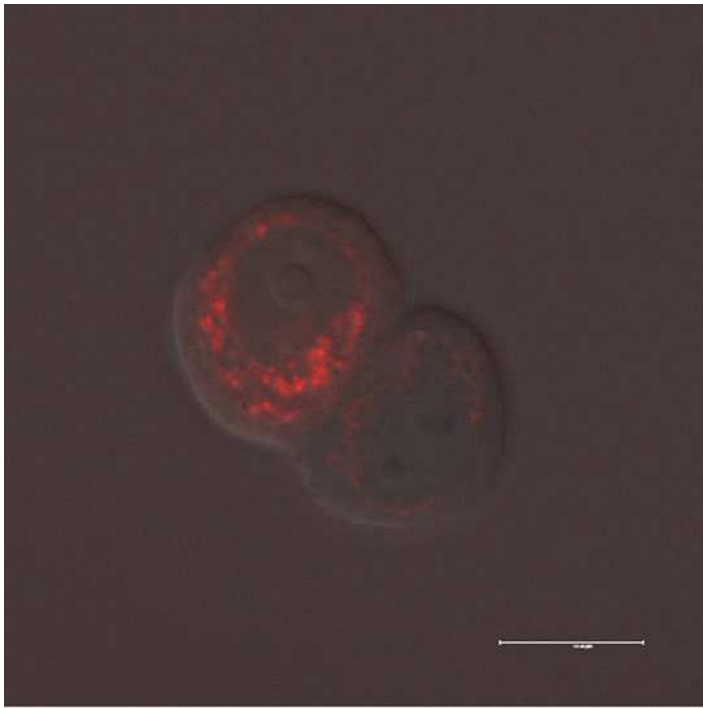


**Fig. 8** Chloromethyl complex 2 in MCF-7 cells showing localisation in organelles. Scale bar=14.4  $\mu\text{m}$

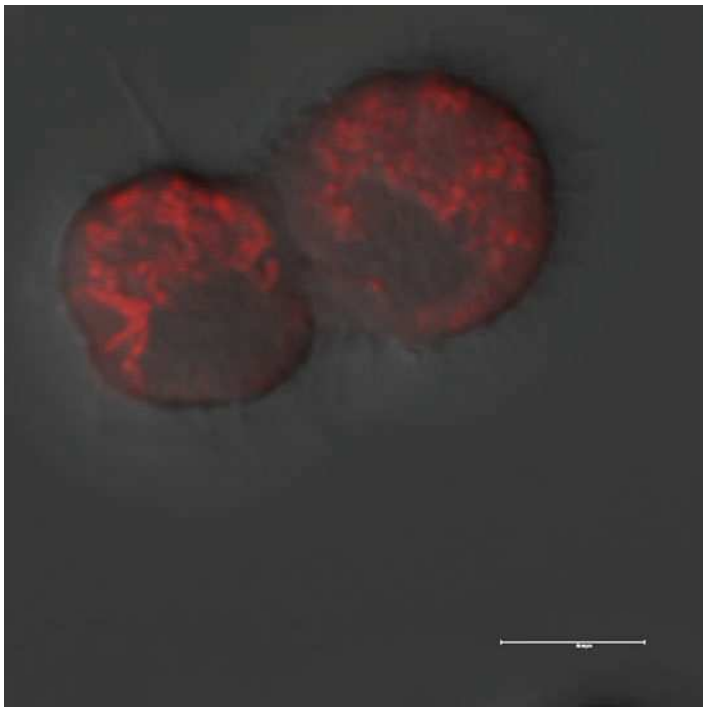


**Fig. 9** TMRE in MCF-7 cells showing localisation in organelles. Scale bar=6.8  $\mu\text{m}$

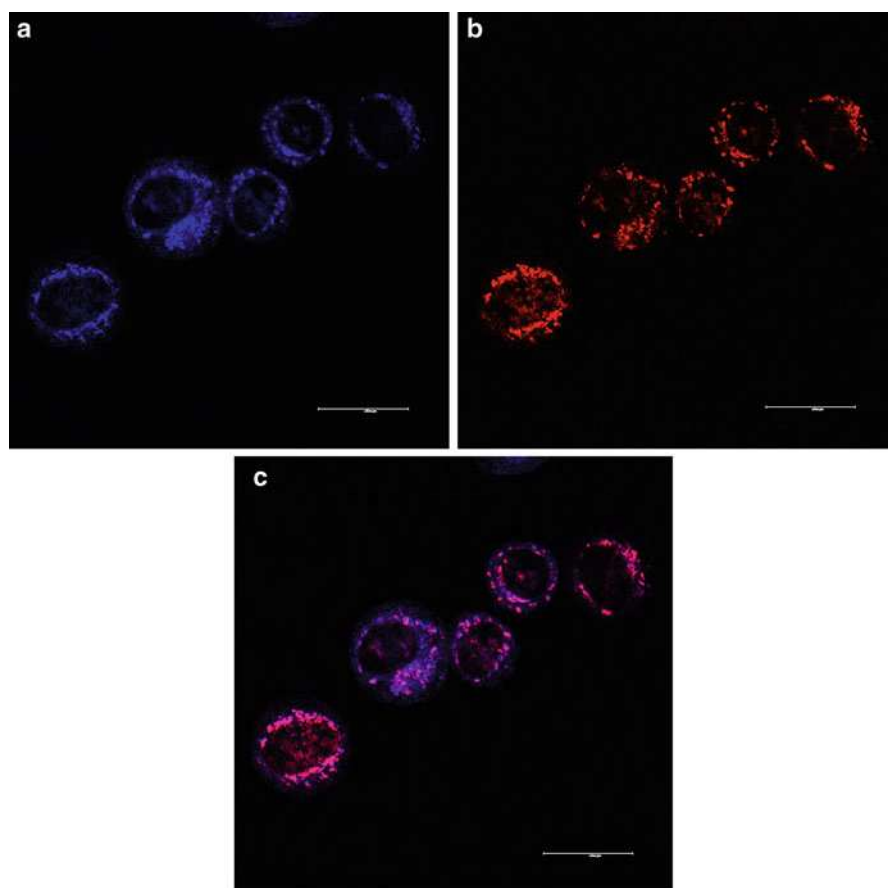


**Fig. 10** Co-localisation of **2** and TMRE in MCF-7 cells. (a) Exciting at 405 nm (selective for **2** over TMRE). (b) Exciting at 543 nm (exclusive for TMRE). (c) Overlay (*purple* = co-localised). Scale bar = 26.5  $\mu\text{m}$

Human adenocarcinoma MCF-7 cells [28] lack the rigid wall of yeast and were selected as a good candidate for assessing the efficacy of the purported mitochondrial-targeting fluorophore **2**. Good uptake was seen (Fig. 8) with >90% of the sample showing luminescence, and a distinctive pattern of localisation in the periphery of the cytoplasm was observed.

Comparison with the localisation shown in the same sample of TMRE (a known mitochondrial-localising fluorophore) [29] showed great similarity to the patterns

shown by **2** (Fig. 9), supporting the proposition that **2** selectively localises in mitochondria.

The mitochondrial localisation of **2** was finally demonstrated by co-localisation experiments (Fig. 10), in which **2** and TMRE were administered to the same sample and differential excitation experiments used to confirm that they had localised in the same compartments of the cells.

Quantification of the co-localisation confirmed that **2** is a selective mitochondrial-targeting fluorophore, to date the most selective  $d^6$ -transition metal luminescent agent designed for a specific biological target to have been demonstrated in fluorescence cell imaging.

### 2.3 *Other Rhenium Polypyridine Complexes in Cell Imaging Applications*

Lo and co-workers have reported the application in cell imaging of a series of sophisticated  $\text{Re}^I$  species bearing biotin and estradiol units, which assist in cell uptake. The biotinylated complexes showed reasonable uptake and localised in zones of the cytoplasm which the authors propose to be the Golgi apparatus [30].

Lo has also reported a dipicolylamine-functionalised rhenium complex, which is responsive to zinc ions, and applied it in cell imaging experiments, showing good uptake and enhancements of emission intensity in the cells upon incubation with zinc or cadmium [31, 32].

### 2.4 *Ruthenium Complexes for Intracellular Oxygen Monitoring Applications*

#### 2.4.1 *Delivery and Utilisation of $\text{O}_2$ in Biological Systems*

A major endeavour of biological research revolves about the measurement and monitoring of  $\text{O}_2$  levels in the environment and within organisms, in their tissues, body fluids and cells [33]. A diversity of methods has been developed and for many purposes successfully deployed for ecological, industrial and biomedical investigations [34]. However, one aspect of these techniques, that of intracellular  $\text{O}_2$  monitoring, remains problematic [35] despite its long history over almost 40 years.

The necessity for reliable intracellular  $\text{O}_2$  determinations has been repeatedly emphasised recently [36, 37]. Living organisms may be regarded as machines that harness the chemistry of  $\text{O}_2$  in a highly controlled and precise series of free energy-conserving reactions. Thus, a potentially catastrophically powerful oxidant is delivered to its sites of use with astonishing efficiency and minimal side reactions. Thus, the air we breathe [20.9%; 21.2 kPa  $\text{O}_2$ ; 158 mmHg; equivalent to 278  $\mu\text{M}$  in water

at 37°C] [38] represents for biological systems a huge excess of  $O_2$ . Thus, when studied in vitro,  $O_2$ -reactive systems of biological origin have highly avid binding characteristics and these become  $O_2$  saturated at much lower partial pressures than ambient. The human  $O_2$ -delivery system [38] displays a series of stepwise decreasing  $O_2$  levels from alveolar air in equilibrium with arterial blood containing the equivalent of 100  $\mu M O_2$ , to the discharge of blood oxyhaemoglobin [depending on  $CO_2$  tension] occurring with the range 80–20 mmHg = 60–30  $\mu M O_2$ , and the working  $pO_2$  is only about 3 mm Hg [39]. The mean  $O_2$  levels within the cells of human tissues are, therefore, less than 0.02 of the ambient atmospheric level. Sites of  $O_2$  utilisation include the mitochondria, peroxisomes and the membranes of the endoplasmic reticulum. Cytochrome *c* oxidase, the binuclear Cu-Fe haemprotein, reacts by way of a multistage cyclic mechanism whereby a concerted and highly efficient 4 electron reduction of  $O_2$  on the inner surface of the inner mitochondrial membrane ( $KmO_2$  of <0.1  $\mu M$ ) leads to a residual steady-state level of  $O_2$  that has not yet been accurately assessed. This can, however, be estimated indirectly by in situ, non-invasive observations of the redox states of respiratory chain components using fluorimetric (for NADPH) and spectrophotometric measurements (for cytochromes) [40, 41]. Several factors influence this  $[O_2]$  in the vicinity of the enzyme: these include those metabolic intermediates that control the activity of the mitochondrial electron transport chain and coupled ATP synthase, i.e. respiratory substrate availability, ADP and inorganic phosphate [20]. Switching between respiratory states occurs on a millisecond timescale so that the dynamics of mitochondrial respiration shows fluctuations on timescales as rapidly as that, as well as in several other slower time domains determined by the ultradian clock, cell division cycle and circadian time [21]. As well as the complete reduction of  $O_2$ , electron transport processes yield low but crucially important partial reduction products ( $OH^-$ ,  $O_2^-$ ,  $H_2O_2$  and singlet  $O_2$ ). These “leaks” of reducing power occur by auto-oxidation of iron–sulphur centres, ubisemiquinone and flavosemiquinones. A minor side reaction of the peroxy-enzyme complex of cytochrome *c* oxidase during the catalytic cycle of its reaction with dioxygen also produces hydrogen peroxide (4). The varied biological functions that have evolved for these “reactive oxygen species” include roles as diverse as signals for synchronised intra- and intercellular mitochondrial coherence [42] and for apoptotic, programmed cell death [43]. In addition to this are the possibilities for widespread oxidative damage to nucleic acids, proteins, lipids, membranes and organelles [44]. At the other membranes where  $O_2$  is consumed, oxidases with less avid binding capabilities reside; thus, the “microsomal” oxidases [e.g. cytochrome P450-dependent mixed function oxidases] have  $KmO_2$  values of about 5–10  $\mu M O_2$  [45] and in peroxisomes, low-affinity flavoenzymes (e.g. D-amino acid oxidase) function alongside catalase.

#### 2.4.2 Probing Intracellular Distributions of $O_2$

The heterogeneous intracellular distribution of these sites of biological oxidation between individual classes of organelles and membranes results in a highly dynamic

pattern of  $O_2$  gradients on a sub-micrometer scale. The “Holy Grail” of cellular physiology is to resolve the complexity of intracellular  $O_2$  distribution by constructing 3-dimensional maps. On a larger scale, the dynamic distribution of  $O_2$  in vivo in body fluids, tissues and organs is an important research aim, and a number of luminophores have been used for this purpose. Examples include porphyrins (Zn protoporphyrin [46], Pd *meso*-tetrakis (4-carboxyphenyl) porphyrin [47] and tetrabenzoporphyrins [48]. In some cell types (e.g. hepatocytes [49]), the concentration of endogenous protoporphyrin IX within mitochondria is sufficient to be used without supplementation for  $O_2$  measurements [50].  $O_2$  is an efficient quencher of electronic excited states in all these examples of phosphorescent luminophores.

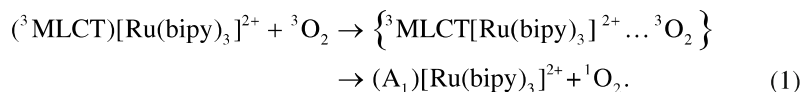
Fluorescence lifetimes of organic fluorophores are mostly of the order of 10–20 ns and the diffusion path of a small molecule is very short. Extra time during which diffusion may occur greatly increases the volume of solution that influences the excited state of each fluorophore molecule [51]. Thus, for some exceptionally long-lived cases [e.g. pyrenebutyric acid (100 ns in air-saturated water)], the  $O_2$ -sensing sphere of influence of the probe is increased from 100 to 1,000 times over that volume affecting the short-lived excited molecules. This exceptionally long-lived fluorescent state has been employed for  $O_2$  mapping in living cells, e.g. in cultured cells of mouse liver by the use of quantitative fluorescence microscopy [52, 53]. The even longer lifetimes provided by phosphorescent luminophores together with their other desirable photophysical properties have led us at Cardiff to employ a Ru coordination complex for the purpose of  $O_2$  measurement within cells [35].

### 2.4.3 Ruthenium Coordination Complexes as $O_2$ Probes

Coordination complexes of  $Ru^{II}$  with polyazaheteroaromatic chelating ligands have attracted much attention as luminophores over the past 40 years due to their interesting spectroscopic, redox and photophysical characteristics, together with the possibility of finely modulating their properties by selection of the type, number and substituents of the heterochromatic chelating ligands of the metal coordination sphere. Excitation of the best-understood Ru complexes is followed by a fast inter-system crossing and the formation of the  $^3MLCT$  excited state. This phosphorescent state (lifetime 0.1–5  $\mu s$  in deoxygenated buffers at room temperature) can participate in a variety of electron and energy transfer reactions with both organic and inorganic species [54]. Quenching by  $O_2$  of the luminescence of a Ru complex was discovered in 1972 [55]; the bimolecular reaction mechanism for the deactivation process has been studied ever since [56, 57]. The intense, broad, 454-nm visible absorption band of  $[Ru(bpy)_3]^{2+}$  and its derivatives is due to an MLCT transition, involving electron transfer from ruthenium-based orbitals to a ligand-centred anti-bonding orbital ( $t_2^5 \pi^{*1}$  configuration) [1]. The allowed nature of this transition advantageously leads to higher absorption coefficients than those associated with formally forbidden  $d-d$  transitions. The luminescent emission transition from the lowest vibrational level of the triplet MLCT excited state then occurs via spin-orbit coupling mediated by the metal, which potentiates rapid and efficient inter-system

crossing over to the triplet states: since emission then occurs from the triplet state, it is of a formally spin-forbidden phosphorescent nature. The photophysical and photochemical characteristics of these inorganic complexes include (a) a lowest excited state that is a charge transfer, thus having photochemical stability rendering them resistant to photobleaching processes; (b)  $d-d$  states well above the emissive states, thereby preventing thermal non-radiative deactivation; (c) high spin-orbit-coupling constants associated with large  $Z$  values, allowing efficient population of emissive triplet states and (d) an emitting state not too low in energy, as this would promote the rate of radiationless decay [1]. “Fine tuning” of these characteristics has been described by substitution of 2,2'-bipyridine and 1,10-phenanthroline with groups of varying steric and electronic character [58].

Most fluorophores are quenched by oxygen, where the relationship between the resultant observed lifetime in oxygenated solution and the fundamental unquenched lifetime is proportional to the degree of quenching (Stern–Volmer). Ruthenium polypyridines and in particular those with extended aromatic substitutions on the coordinated diimine, which reduce solvent perturbations, are particularly prone to luminescence quenching by dioxygen as there is an efficient, diffusion-controlled, collisional interaction between the triplet MLCT excited state of the ruthenium polypyridyl and the triplet ground state of dioxygen, leading to the formation of the ground state of the ruthenium polypyridyl and singlet dioxygen (1) [58]



Thus, the excited-state lifetime of a ruthenium polypyridyl species is exquisitely sensitive to oxygen concentration due to the efficiency associated with a diffusion-controlled quenching process leading to a very high rate of deactivation of the excited-state species and a concomitant drop in the average luminescence lifetime.

Singlet oxygen formation by energy transfer from the  $^3\text{MLCT}$  excited state to the dioxygen molecule [59] as well as predominant electron-transfer quenching that produces superoxide anion [60] have both been described.

For  $\text{O}_2$ -sensing purposes,  $\text{Ru}^{2+}$  complexes show many advantages [61, 62]. A range of coordinating ligands have been tested in a series of  $[\text{RuL}_3]$  complexes, where  $L$  was 2,2'-bipyridine (bpy); 1,10-phenanthroline (phen); 2,2'-bipyrazine (bpz); 4,7-diphenyl-1,10-phenanthroline-4,7 sulphonate (dpds) or 1,10-phenanthroline-5-octadecanamide (poda) [56]. Solvent effects on the  $\text{O}_2$  quenching process were also studied by measuring rate constants ( $kq$ ) for the quenching of the  $^3\text{MLCT}$  state by dioxygen and quantum yields ( $\phi_\Delta$ ) of singlet oxygen production in aqueous or methanolic reaction mixtures. The sole pathway for quenching of the excited  $[\text{RuL}_3]$  complexes by dioxygen in methanol was energy transfer, whereas in water, higher quenching rate constants but lower values of  $\phi_\Delta$  were observed. Most importantly, complexes based on the 4,7-diphenyl-1,10-phenanthroline ligand proved very efficient and stable singlet-oxygen sensitizers with  $\phi_\Delta$  values close to unity in air-saturated MeOH [62].

#### 2.4.4 Recent Advances in O<sub>2</sub> Mapping

Singlet oxygen O<sub>2</sub>(a<sup>1</sup>Δg) can itself be detected as being heterogeneously distributed in single cells; its differential quenching rates in different intracellular locales is not as important as the diffusion rate constants [63, 64]. The importance of the determination of this component lies in its signalling functions as well as its deleterious effects as a powerful oxidant of cellular components that lead to necrosis and/or apoptosis. Phosphorescence at 1,270 nm has been used extensively over the past 25 years. Photosensitisers (e.g. 5, 10, 15, 20 tetra-kis(*N*-methyl-4-pyridyl) 21H,23H-porphyrine) have been used to promote singlet oxygen generation upon pulsed laser irradiation, and intracellular lifetime measurements in single cells give values of 3 μs, as well as in sucrose solutions of varying viscosities and of 3.5 μs in water. This gives a spherical spatial domain of radius ~100 nm for intracellular activity [65].

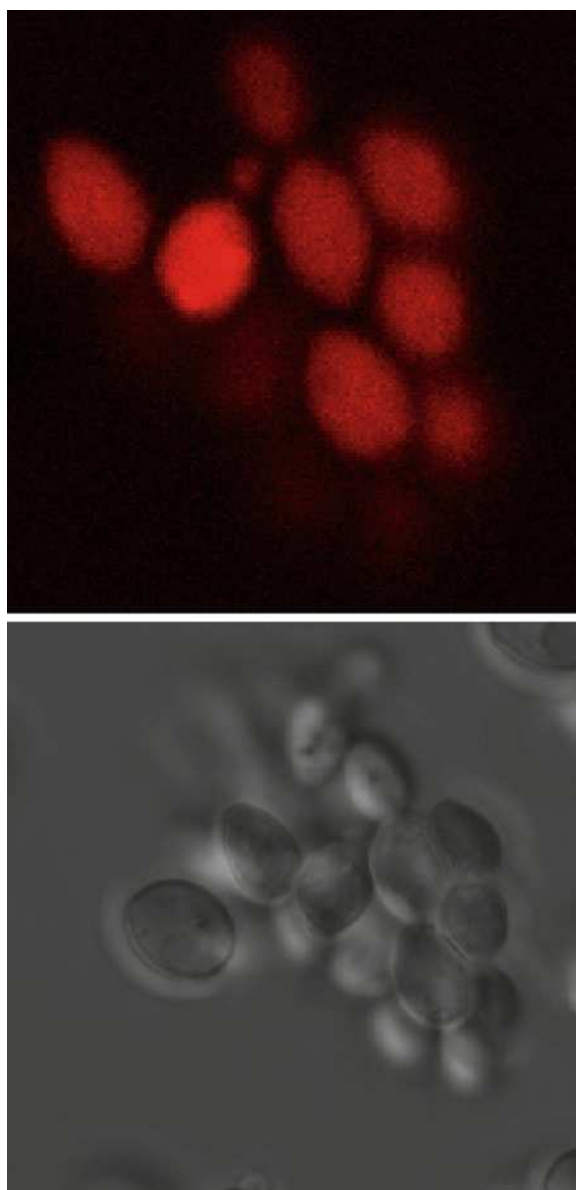
Some limitations of the phosphorescence quenching method for mapping O<sub>2</sub> in tissues have been pointed out [66] and these have been overcome by the use of energy capture by a probe with several two-photon absorption antennae [67]. Thereby, the low two-photon absorption cross sections of some typical phosphorescent probes based on Pt and Pd porphyrins are enhanced. The successful use of PtP-C343 (consisting of a ~5-nm diameter phosphorescent Pt-*meso*-tetra-arylporphyrin core, several coumarin – 343 units, a polyarylglycine dendrimer and peripheral oligoethylene-glycol residues) efficiently captures excitation energy for transmission by Förster-type resonance energy transmission to the O<sub>2</sub>-quenchable emitter and prevents interactions with proteins and other biological solutes, respectively. It has been shown that quenching plots are unaffected by pH changes or cell growth media containing albumin, whereas these of unprotected porphyrins are drastically altered.

#### 2.4.5 Encapsulation of a Ruthenium Coordination Complex into Nanoparticles

Immobilisation [68] or encapsulation [69–72] in polymeric materials provides possibilities for minimisation of toxicity and invasive perturbation of biological systems. Some observed disadvantages of Ru coordination complexes used in aqueous solution [73], but without prior encapsulation, include minimal uptake into cells, toxic effects on metabolism survival and proliferation of cells and organisms and non-specific binding to proteins and membranes [74, 75]. In our present work, we show that further extension of these fundamental principles permits the fabrication of nanoscale O<sub>2</sub> sensor particles that, when electroporated into yeast or animal cells, report local O<sub>2</sub> concentrations and rapidly sense changes during aerobic–anaerobic shifts in the extracellular environment, avoiding some of the problems associated with non-encapsulated Ru coordination complex in biological imaging applications.



**Fig. 11** Images of *Saccharomyces cerevisiae*. *Upper panel*, luminescence. *Lower panel*, Nomarski differential interference contrast. Leica TCS SP2 AOBS confocal microscopy using a  $\times 40$  objective with  $\times 2.85$  zoom, with excitation at 514 nm and detection at 520–600 nm



#### 2.4.6 Imaging Applications of a Nanoparticle-Encapsulated Ruthenium Complex

Quenching of the triplet excited-state lifetime of the Ru complex within the acrylamide-based nanoparticles is strongly determined by collision with  $O_2$  molecules. Thus, it is only those  $O_2$  molecules within the diameter/boundaries of the nanoparticles that are sensed and it is only local  $O_2$  levels that are reported [69, 70].

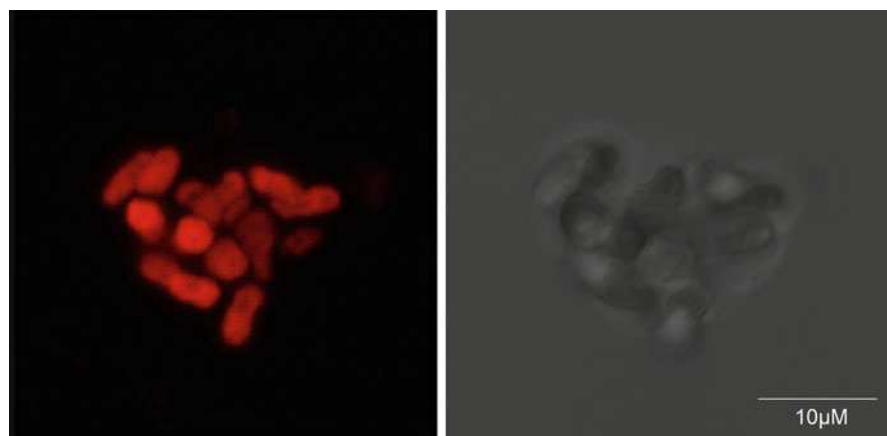


**Fig. 12** Images of *Schizosaccharomyces pombe*. *Left*, luminescence. *Right*, Nomarski differential interference contrast. Confocal microscopy was as in Fig. 11

Consequently, increased  $O_2$  concentrations give increased rates of phosphorescence quenching, giving correspondingly decreased total phosphorescence intensities and shorter phosphorescence lifetimes [56]. Both phosphorescence intensities and lifetimes are highly sensitive to solvent effects and/or binding to proteins/membranes due to restriction of vibrational freedom and consequently diminished quantum yields. However, embedding of the luminophore within the polyacrylamide particle minimises its interactions with solvent and cellular constituents.

#### 2.4.7 Incorporation into Yeast Cells

When baker's yeast, the budding *S. cerevisiae*, was electroporated in the presence of the nanoparticles using  $3 \times 450$  V pulses (960  $\mu$ F capacitance, 200  $\Omega$  resistance), most of the organisms showed extensive labelling with the luminophore when examined by confocal microscopy as evident by comparison with the Nomarski differential interference contrast image of the identical observation field (Fig. 11).

The basis for the population heterogeneity of uptake was not investigated, but it seems that the cell walls of some of these organisms provide barriers to penetration. Where the nanoparticles had entered the organisms, luminescence labelling was intense and uniform throughout the cytoplasm, and within cellular inclusions and organelles, but cell walls were not phosphorescent.

Quite a different result was obtained after an identical electroporation treatment of the fission yeast *Schizosaccharomyces pombe*, where samples were taken from a growing culture (Fig. 12). In this case, every organism became labelled irrespective of the cell division cycle phase: hence, short (7  $\mu$ m) and longer (up to 14  $\mu$ m) rod-shaped stages showed intense luminescence, including those with transverse septa

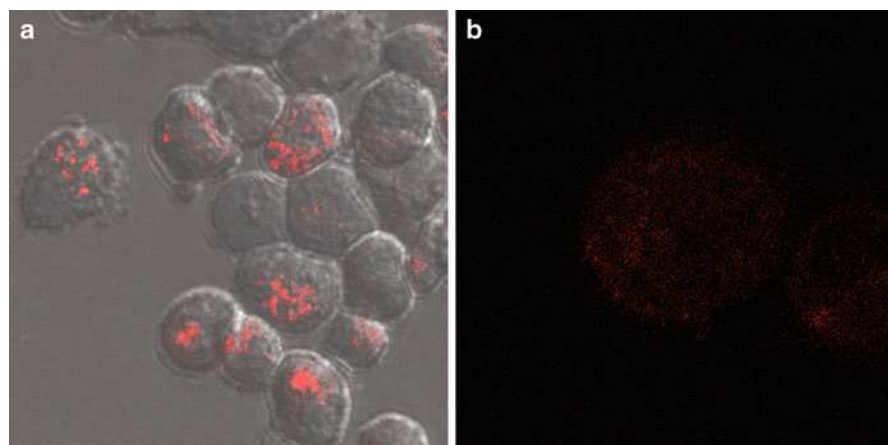


**Fig. 13** Images of MCF-7 cells. Cells were about 12- $\mu\text{m}$  diameter. Confocal microscopy was as in Fig. 11. (a) Non-electroporated cells: Nanoparticles incorporated by spontaneous endosomal uptake (luminescent image overlaid by corresponding Nomarski differential interference contrast image). (b) Two electroporated cells showing more uniformly dispersed intracellular nanoparticle distributions than in the cells in (a), where accumulation was by endosomal uptake

**Table 3** Luminescence lifetimes of nanoparticles and MCF-7 cells

	Luminescence lifetime ( $\mu\text{s}$ )
Ru nanoparticles in air	1.81
Ru nanoparticles in dinitrogen	4.02
Electroporated cells in air	2.92
Electroporated cells in dinitrogen	4.06

about to undergo cell division by fission. (Organisms showing spherical or elliptical profiles are images produced as a consequence of optical sectioning).

#### 2.4.8 Incorporation into a Cultured Human Cell Line

Highly uniform uptake was observed throughout populations of human MCF-7 cells grown in culture and in this case, electroporation was not necessary for the uptake. Exposure for 15 min to nanoparticles produced cells, which contain endosomal vacuoles, that accumulated nanoparticles as dense clusters (Fig. 13a). Electroporation ( $3 \times 320 \text{ V}$ ) yields a much more uniform and diffusely labelled luminophore distribution (Fig. 13b). Here, it is evident that, in addition to clusters of aggregated particles, a more diffuse background of cytoplasmic and organellar luminescence occurred.

The free Ru-embedded acrylamide nanoparticles were photophysically assessed in aerated 1.0 M sorbitol. The luminescence properties were typical of  $^3\text{MLCT}$ -emitting species of the generic-related type  $\{\text{Ru}(\text{phen})_3\}^{2+}$  with a broad structureless band observed at ca. 608 nm following excitation at 450 nm (i.e. selective irradiation

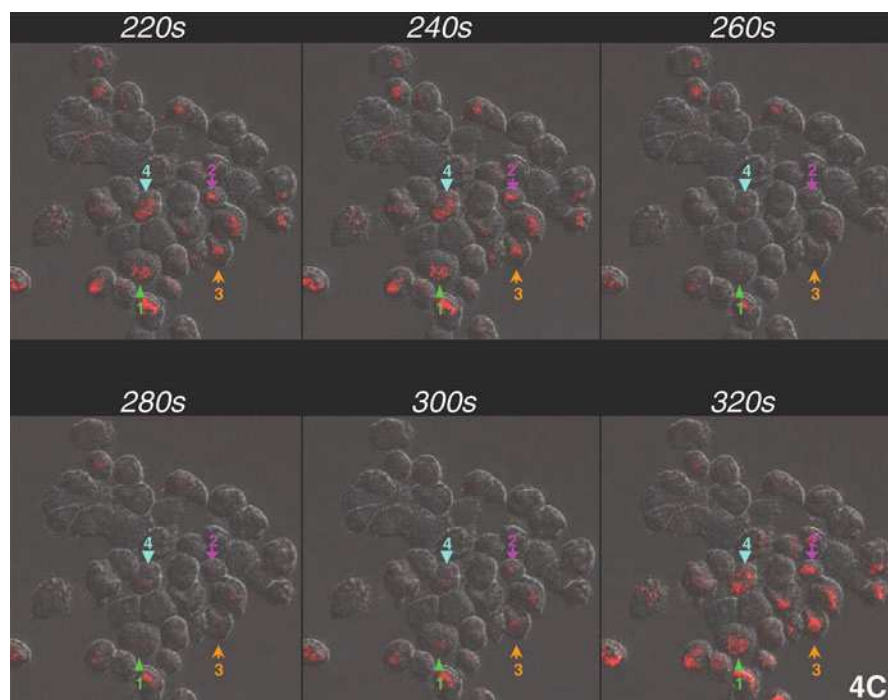


**Fig. 14** Time series of images of MCF-7 cells labelled with nanoprobe and equilibrated in an atmosphere of dinitrogen (220 and 240 s) and then air (until 280 s) before switching back again to anaerobic conditions

of the  $^1\text{MLCT}$  transition). The luminescence lifetime of the 608-nm band was  $1.81\ \mu\text{s}$  ( $4.02\ \mu\text{s}$  under a dinitrogen atmosphere) compared to free  $[\text{Ru}(\text{dpp}(\text{SO}_3\text{Na})_2)_3]\text{Cl}_2$  in water (lifetimes of  $0.93$  and  $3.7\ \mu\text{s}$  for aerated and argon atmospheres, respectively [73]), suggesting that the acrylamide nanoparticle shell enhances the photophysical properties of the embedded Ru luminophores.

Luminescence lifetime measurements (Table 3) were obtained on a range of cells following different treatment regimes (electroporation versus controls, i.e. non-electroporated human MCF-7 cells) and air atmosphere versus dinitrogen. Comparison, in air, of the electroporated cells with the freely suspended nanoparticles revealed that the emission lifetime of the probe was dramatically lengthened reflecting the oxygen-depleted intracellular environment due to respiratory activity. The intracellular probe was also found to be sensitive to changes in external atmospheric levels of oxygen; long-term depletion resulted in a luminescence lifetime comparable to that of the free nanoparticles in an oxygen-free atmosphere. Interestingly, restoration of the aerobic atmosphere led to a dramatic shortening of the lifetime ( $1.86\ \mu\text{s}$ ) before returning to ca.  $2.9\ \mu\text{s}$  after about 5 min. This is difficult to rationalise as a purely chemical process, as the effect of increased oxygen concentration would be essentially instantaneous and must reflect a change in the

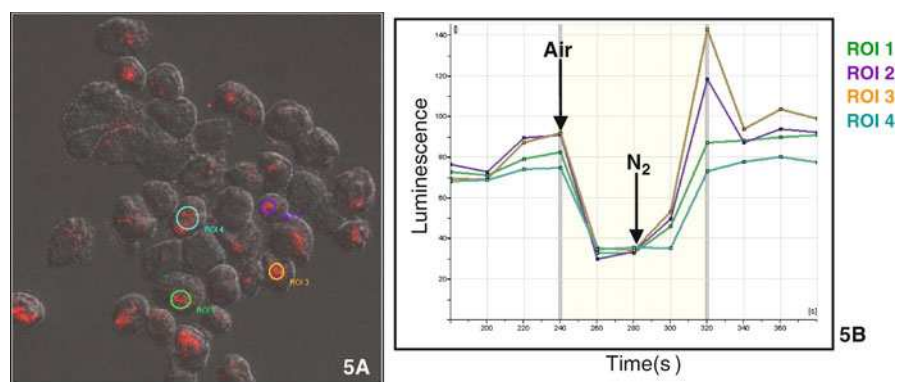


**Fig. 15** Luminescence of selected areas of anaerobic individual cells during an aerobic pulse

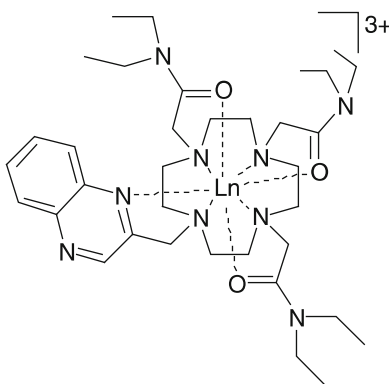
biochemistry of the cell compartment containing the nanoparticles. Possibly, the initial shortening is indicative of rapid delivery of oxygen to the nanoparticle-rich domains, which have shut down respiration due to the low oxygen concentration, leading to hyperoxic conditions and a short lifetime, followed by slower restoration of oxygen-consuming processes which restore the equilibrium values as oxygen concentration reverts to typical values.

Figure 14 shows a series of images of MCF-7 cells showing changes of luminescence intensities at 20-s intervals, as obtained while changing the gaseous phase within the observation chamber of the confocal microscope. Initially, the cells immersed in a thin layer of 1.0 M sorbitol were dinitrogen equilibrated (frames at 220 and 240 s). Then, the mobile gas phase was switched to air, and by 260 s emission intensities in most of the cells were greatly diminished. Restoration of dinitrogen (just after the 280-s scan) reversed these changes.

Luminescence of selected areas within four cells (Fig. 15a) is plotted separately as time courses (Fig. 15b) and these indicate overall similarities between individuals, except that two cells showed an overshoot of emission intensity before re-attaining steady-state anaerobic levels.

These data indicate the feasibility of using a polyacrylamide-embedded Ru coordination complex as an  $O_2$  nanoprobe for biological imaging. Advantages of this approach include minimisation of direct exposure of the sensing molecules to perturbative physical and chemical intracellular local environments or leakage [76] without restriction of access by gases. Use of fluorescence lifetime rather than intensity imaging promises further improved sensitivity and removal of ambiguities of interpretation due to heterogeneity of local conditions [77, 78]. Lifetime imaging of long-lived emission processes is not straightforward with all commercially available laser scanning confocal microscopes, but more recent models with fluorescence lifetime imaging software [79] allow imaging in the microsecond emission lifetime domain. Alternatively, a pinhole shifting method for collecting long-lifetime phosphorescence has recently been described that can be used with

**Fig. 16** Quinoxaline-functionalised macrocyclic triamide Ln(III) complex



more generally available instrumentation and could be used for the application described here [80].

### 3 Development and Application of Novel Lanthanide Ion Luminophores

Due to the forbidden nature of  $f-f$  electronic transitions, a general design strategy is required when synthesising emissive lanthanide complexes: a sensitising chromophore (often referred to as an antenna that can be organic or inorganic in nature) is required to facilitate effective population (usually, but not exclusively, via energy transfer) of the lanthanide excited state, circumventing the inherently poor molar absorptivity of these ions [81]. Briefly, it is important to note that the heavy lanthanide ion promotes effective inter-system crossing and the final donor state of the chromophore is often triplet in nature. Although this does not preclude energy transfer from a singlet excited state, a consideration of the relative energies of the chromophore-centred excited states with respect to the accepting lanthanide-ion excited state is important in the design of novel luminophores. The specific details and complexities of this process have been detailed elsewhere [82, 10]. The quantum yields of sensitised lanthanide-ion complexes can be quite low (<1%), particularly those associated with near-IR emission, and strategies associated with maximising both quantum yield and luminescence lifetime generally involve minimising the proximity of quenching vibrational manifolds of O-H, N-H and C-H oscillators [83].

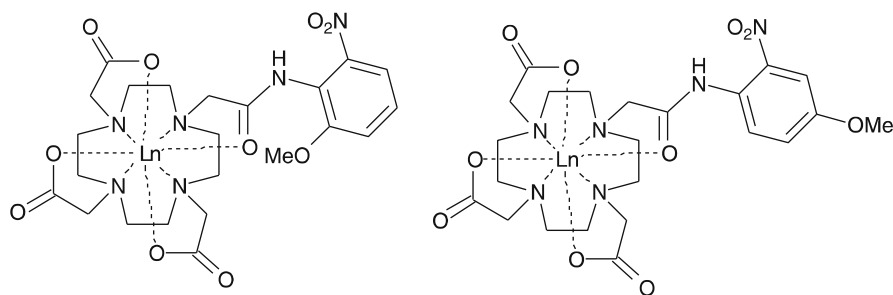


**Fig. 17** Ln(III) complex appended with *N*-(2-nitrophenyl)acetamide-derived chromophores

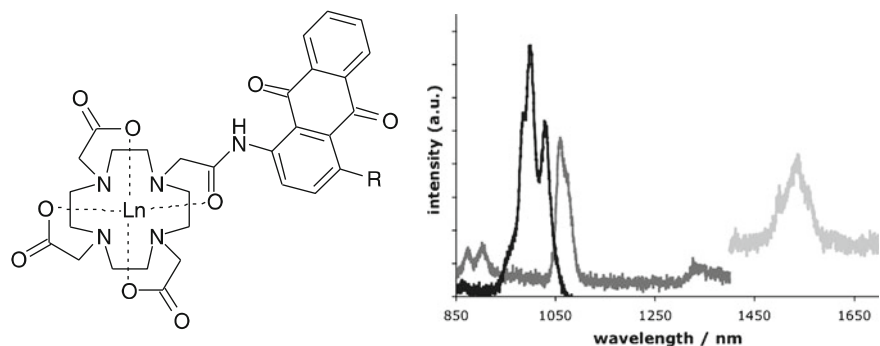


**Fig. 18** Anthraquinone-appended complexes (*left*). Near-IR emission from Yb(III), Nd(III) and Er(III) following sensitisation at 450 nm (in D<sub>2</sub>O)

### 3.1 Development of Near-IR-Emissive Lanthanide-Ion Luminophores

The development of new chromophores for sensitised lanthanide emission in the near IR is ongoing and crucial to the continued development of useful complexes for imaging applications. Examples of ligand frameworks suitable for the formation of kinetically stable lanthanide complexes in aqueous solution include either cyclen architectures or DTPA-type structures as well as polydentate heterocyclic ligands. Aromatic moieties, such as pyrene [84], and heterocycles, such as quinoxaline (Fig. 16) [85], can sensitise Nd(III), Er(III) and Yb(III) in either aqueous or methanolic solutions. In the latter case, the cyclen framework was functionalised as a lipophilic triamide. The complexes also showed pH-dependent emission properties as a result of the protonatable nitrogen atoms within the quinoxaline unit.

Judicious functional group substitution allows simple phenyl-based derivatives to absorb into the visible region while demonstrating sensitisation of Nd(III) and Yb(III): aryl-substituted *N*-(2-nitrophenyl)acetamide-derived chromophores can be



incorporated into DO3A frameworks (Fig. 17) [86]. A combined structural and spectroscopic study, supported with DFT calculations, showed that the absorption properties of the chromophores are dictated by the extent of electronic delocalisation throughout the aryl unit, which in turn was determined by the position of the aryl substituents.

The biological and medicinal importance of functionalised 9,10-anthraquinone species has been demonstrated through their DNA-targeting behaviour [87], cytotoxicity (delivering anti-cancer, anti-malarial and anti-angiogenic properties) [88, 89] and their potential in Alzheimer's disease treatment via inhibition of tau protein aggregation [90]. Generally, substituted anthraquinones possess high-molar-absorption coefficients that can be tuned, by choice of substituents, throughout the visible spectral region. In particular, amino-substituted anthraquinones possess red-shifted absorption profiles, which are attributed to significant intramolecular charge transfer (ICT) character (formally, N-to-quinone). We have developed the use of anthraquinone units as effective antennae for sensitised Ln(III) emission (Fig. 18) [91]: two novel anthraquinone-derived macrocyclic ligands (**L1** via 1-amino-9,10-anthraquinone and **L2** via 1-amino-4-hydroxy-9,10-anthraquinone) have been reported together with their corresponding Ln<sup>III</sup> complexes, **Ln-L1/2** (Ln = Nd<sup>III</sup>, Gd<sup>III</sup>, Er<sup>III</sup>, Yb<sup>III</sup>) [86]. Both **Ln-L1** ( $\lambda_{\text{max}} \approx 380$  nm) and **Ln-L2** ( $\lambda_{\text{max}} \approx 450$  nm) complexes absorb in the visible region with good extinction coefficients ( $\epsilon_{\text{vis}} > 2 \times 10^3 \text{ M}^{-1} \text{ cm}^{-1}$ ). Steady-state and time-resolved measurements showed that the anthraquinone units sensitise Nd<sup>III</sup>, Er<sup>III</sup> and Yb<sup>III</sup> ions. Deprotonation of the 4-hydroxyl group of L2 resulted in a significant bathochromic shift in the absorption profile, allowing sensitised near-IR emission utilising visible light  $\lambda_{\text{ex}} = 575$  nm.

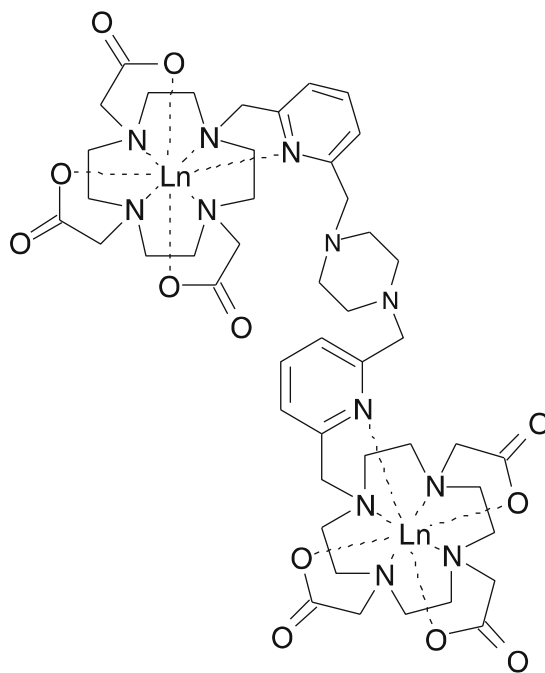
### 3.2 Development of Responsive Lanthanide Complexes

Lanthanide-ion complexes can be exploited in the design of molecular probes towards biologically important analytes [92]. One approach in the design of responsive lanthanide complexes is based upon exploiting changes in the inner-sphere hydration of the lanthanide ion. Subtle modulation of inner-sphere hydration (ideally, without compromising the kinetic stability of the complex) can induce detectable changes in *f*-centred luminescence. This is particularly pertinent when considering the emission from Eu<sup>III</sup>, which possesses hypersensitive transitions, allowing coordinative changes at the metal to be probed.

Zinc is a metal of fundamental neurobiological and neuropathological importance [93]. Consequently, an understanding of its role in such contexts requires an ability to detect, track and image zinc ions. The physical and electronic nature of Zn<sup>II</sup> dictates that biological imaging of it is dominated by two main modes: optical fluorescence and magnetic resonance imaging. The probe complex was designed to be luminescently responsive to Zn<sup>II</sup> in the presence of a competitive ionic mixture at pH 7.4 [94]. The structure of the complex is based upon a carboxylate, functionalised azamacrocyclic and possesses a chromophoric bis-picoyl unit for binding Zn<sup>II</sup>.



**Fig. 19** Lanthanide probes with luminescence and magnetic relaxivity responses



The effect on both ligand fluorescence and  $\text{Eu}^{\text{III}}$  phosphorescence was investigated in the presence and absence of  $\text{Zn}^{\text{II}}$ . The study revealed that binding  $\text{Zn}^{\text{II}}$  increased the intensity of ligand fluorescence and modulated the inner-sphere hydration number of  $\text{Eu}^{\text{III}}$  ( $q$  increases from 0 to 2). The change in coordination environment induced pronounced changes in the form of the steady-state spectra (Fig. 19) and reduced the lifetime of the  $\text{Eu}(\text{III})$  emission from 1 to 0.4 ms in water, allowing the presence of  $\text{Zn}^{\text{II}}$  to be signalled by changes in both emission intensity and lifetime.

This methodology has been extended to a new piperazine-bridged bis-macrocyclic ligand, which gave the dimetallic complexes (Fig. 19:  $\text{Ln} = \text{Gd}^{\text{III}}, \text{Eu}^{\text{III}}$ ) aimed towards providing probes with both luminescence and magnetic relaxivity responses [95]. The interaction of  $\text{Cu}^{\text{II}}$  and  $\text{Hg}^{\text{II}}$  with the lanthanide complexes was probed using luminescence and relaxivity measurements. Addition of  $\text{Cu}^{\text{II}}$  resulted in quenching of the  $\text{Eu}^{\text{III}}$  emission, but no increase in longitudinal proton relaxivity ( $r_1$ ) of the  $\text{Gd}^{\text{III}}$  dimer. In contrast, addition of  $\text{Hg}^{\text{II}}$  (10 eq.) caused changes to the emission bands of  $\text{Eu}^{\text{III}}$  and shortened lifetime in water, together with an approximate 20% increase in  $r_1$  of the  $\text{Gd}(\text{III})$  dimer to  $10.3 \text{ mM}^{-1} \text{ s}^{-1}$  (30 MHz,  $25^\circ\text{C}$ ) suggesting a net increase in hydration at the  $\text{Ln}^{\text{III}}$  centres upon binding of  $\text{Hg}^{\text{II}}$ .

Investigations into the possibilities of modulating near-IR emission [96] have also been undertaken using crown ether-appended ditopic cryptate-type ligands. Binding an alkali metal ion in the crown ether portion of the ligand alters the absorption profile (dominated by ligand-centred  $\pi \rightarrow \pi^*$ ) of the complex, thus allowing transduced variations in near-IR emission intensity from the reporting  $\text{Nd}(\text{III})$  ion.

## 4 Conclusion

It is now very clear, through recent developments, that the use of metalcontaining luminophores in a biological context provides an important and valuable consideration for informative cellular imaging. Such species can offer great flexibility in terms of both photophysical attributes and targeting of specific intracellular compartments, a crucial attribute when elucidating details of cell function. Emissive *d*- and *f*-block complexes not only provide numerous photophysical advantages over organic fluorophores, but also offer great scope in the design of responsive probes that can relay information on analyte concentrations and environmental changes in a biological context.

**Acknowledgements** Collaborators in Cardiff who cultured organisms and cells, synthesised new luminophores and obtained optical images were Dr. Anthony J. Hayes, Dr. Jonathan B. Court, Dr. Coralie O. Millet, Dr. Victoria Gray, Dr. Vanesa Fernandez-Moreira, Dr. Sion H. Lloyd, Ms. Flora L. Thorp-Greenwood Dr. Michael Andrews, Ms. Jennifer E. Jones, Ms. Catrin F. Williams and Mr. Marc Isaacs. Expert advice and preparations of nanoparticles were provided by Dr. Lars Folke Olsen, Dr. Allan Poulsen and Ms. Anita Lunding of the University of Southern Denmark at Odense.

## References

1. DeGraff BA, Demas JN (2005) Luminescence-based oxygen sensors. In: Geddes J and Lakowicz JR (eds) Reviews in fluorescence, vol 2. Springer, New York, pp 125–151
2. Amoroso AJ, Coogan MP, Dunne JE, Fernández-Moreira V, Hess JB, Hayes AJ, Lloyd D, Millet CO, Pope SJA, Williams C (2007) Rhenium *fac*-tricarbonyl bisimine complexes: biologically useful fluorochromes for cell imaging applications. *Chem Commun* 29:3066–3068
3. Amoroso AJ, Arthur RJ, Coogan MP, Court JB, Fernández-Moreira V, Hayes AJ, Lloyd D, Millet CO, Pope SJA (2008) 3-Chloromethylpyrididyl bipyridine *fac*-tricarbonyl rhenium: a thiol-reactive luminophore for fluorescence microscopy accumulates in mitochondria. *New J Chem* 32:1097–1102
4. Lo KK, Louie M, Sze K, Lau J (2008) Rhenium(I) polypyridine biotin isothiocyanate complexes as the first luminescent biotinylation reagents: synthesis, photophysical properties, biological labelling, cyto toxicity and imaging studies. *Inorg Chem* 47:602–611
5. Lo KK, Lee TKM, Lo JSY, Poon WL, Cheng SH (2008) Luminescent biological probes derived from ruthenium (II) estradiol polypyridine complexes. *Inorg Chem* 47:200–208
6. Yu M, Zhao Q, Shi L, Li F, Zhou Z, Yang H, Yi T, Huang C (2008) Cationic iridium (III) complexes for phosphorescence staining in the cytoplasm of living cells. *Chem Commun* 18:2115–2117
7. Montgomery CP, Murray BS, New EJ, Pal R, Parker D (2009) Cell-penetrating metal complex optical probes: targeted and responsive systems based on lanthanide luminescence. *Accounts Chem Res* 42:925
8. Bünzli JCG, Chauvin AS, Vandevyver CDB, Bo S, Comby S (2008) Lanthanide bimetallic helicates for in vitro imaging and sensing. *Fluorescence methods and applications: spectroscopy, imaging, and probes*. Book series. *Ann N Y Acad Sci* 1130:97
9. Botchway SW, Charnley M, Haycock JW, Parker AW, Rochester DL, Weinstein JA, Williams JAG (2008) Time-resolved and two-photon emission imaging microscopy of live cells with inert platinum complexes. *Proc Natl Acad Sci USA* 105:16071

10. Eliseeva SV, Bünzli JCG (2010) Lanthanide luminescence for functional materials and bio-sciences. *Chem Soc Rev* 39:189
11. Faulkner S, Pope SJA, Burton-Pye BP (2005) Lanthanide complexes for luminescence imaging applications. *Appl Spec Rev* 40:1
12. Lowry MS, Hudson WR, Pascal RA, Bernhard S (2004) Accelerated luminophore discovery through combinatorial synthesis. *J Am Chem Soc* 126:14129–14135
13. Stufkens DJ, Vlcek A Jr (1998) Ligand-dependent excited state behaviour of Re(I) and Ru(II) carbonyl–diimine complexes. *Coord Chem Rev* 177:127–179
14. Juris A, Balzani V, Barigellatti F, Campagna S, Belser P, von Zelewsky A (1998) Ru(II) Polypyridine complexes: photophysics, photochemistry, electrochemistry, and chemiluminescence. *Coord Chem Rev* 84:85–227
15. Beer PD, Hayes EJ (2003) Transition metal and organometallic anion complexation agents. *Coord Chem Rev* 240:167–189
16. Kneas KA, Xu W, Demas JN, DeGraff BA, Zipp AP (1998) Luminescence-based oxygen sensors:  $\text{ReL}(\text{CO})_3\text{Cl}$  and  $\text{ReL}(\text{CO})_3\text{CN}$  complexes on copolymer supports. *J Fluoresc* 8:295–300
17. Reitz GA, Demas JN, DeGraff BA, Stephens EM (1998) Inter- and intramolecular excited-state interactions of surfactant-active rhenium(I) photosensitizers. *J Am Chem Soc* 110:5051–5059
18. Coogan MP, Fernandez-Moreira V, Hess JB, Pope SJA, Williams C (2009) Rhenium fac-tricarbonyl bisimine complexes: luminescence modulation by hydrophobically driven intramolecular interactions. *New J Chem* 33:1094–1107
19. Coogan MP, Fernández-Moreira V, Kariuki BM, Pope SJA (2009) Thorp-Greenwood, F.L. A rhenium tricarbonyl 4'-oxo-terpy trimer as a luminescent molecular vessel with a removable silver stopper *Angew. Chem Int Ed Eng* 48:4965–4968
20. Mullice LA, Pope SJA (2010) The development of responsive, luminescent lifetime probes based upon axially functionalised fac-[ $\text{Re}(\text{CO})_3(\text{di-imine})(\text{L})$ ]<sup>+</sup> complexes. *Dalton Trans* 39:5908–5917
21. Stephenson KA, Banerjee SR, Besenger T, Sogbein OO, Levadala MK, McFarlane N, Lemon JA, Boreham DR, Maresca KP, Brennan JD, Babich JW, Zubieta J, Valliant JF (2004) Bridging the gap between in vitro and in vivo imaging: isostructural Re and <sup>99m</sup>Tc complexes for correlating fluorescence and radioimaging studies. *J Am Chem Soc* 126:8598
22. Liu S, Edwards DS (1999) <sup>99m</sup>Tc-labeled small peptides as diagnostic radiopharmaceuticals. *Chem Rev* 99:2235–2268
23. Viola-Villegas N, Rabideau AE, Bartholoma M, Zubieta J, Doyle RP (2009) Targeting the cubilin receptor through the vitamin B<sub>12</sub> uptake pathway: cytotoxicity and mechanistic insight through fluorescent Re(I) delivery. *J Med Chem* 52:5253–5261
24. Fernandez-Moreira V, Thorp-Greenwood FL, Coogan MP (2010) Application of *d*<sup>6</sup> transition metal complexes in fluorescent cell imaging. *Chem Commun* 46:186–202
25. Minamikawa T, Sriratana A, Williams DA, Bowser J, Hill S, Nagley P (1999) Chloromethyl-X-rosamine (MitoTracker Red) photosensitises mitochondria and induces apoptosis in intact human cells. *J Cell Sci* 112:2419–2430
26. Dattelbaum JD, Abugo OO, Lakowicz JR (2000) Synthesis and characterization of a sulfhydryl-reactive rhenium metal–ligand complex. *Bioconjug Chem* 11:33–536
27. Castellano FN, Dattelbaum JD, Lakowicz JR (1998) Long-lifetime Ru(II) complexes as labeling reagents for sulfhydryl groups. *Anal Biochem* 255:165–170
28. Soule HD, Vazquez J, Long A, Albert S, Brennan M (1973) (1973) A human cell line from a pleural effusion derived from a breast carcinoma. *J Natl Cancer Inst* 51:1409–1413
29. Whitaker JE, Moore PL, Haugland RP, Haugland RP (1991) Dihydratotetramethylrosamine: a long wavelength, fluorogenic peroxidase substrate evaluated in vitro and in a model phagocyte. *Biochem Biophys Res Commun* 175:387–393
30. Lo KK-W, Louie M-W, Lau SK-S, S-Y J (2008) Rhenium(I) polypyridine biotin isothiocyanate complexes as the first luminescent biotinylation reagents: synthesis, photophysical properties, biological labeling, cytotoxicity, and imaging studies. *Inorg Chem* 47:602–611
31. Louie MW, Lam MH-C, Lo KK-W (2009) Luminescent polypyridinerhenium(I) bis-biotin complexes as crosslinkers for avidin. *Eur J Inorg Chem* 28:4265–4273

32. Louie M-W, Liu H-W, Lam MH-C, Lau T-C, Lo KK-W (2009) Novel luminescent tricarbonylrhenium(I) polypyridine tyramine-derived dipicolylamine complexes as sensors for zinc(II) and cadmium(II) ions. *Organometallics* 28:4297–4307
33. Lloyd D (2002) Noninvasive methods for the investigation of organisms at low oxygen levels. *Adv Appl Microbiol* 51:155–183
34. Gnaiger E, Forstner H (eds) (1983) *Polarographic oxygen sensors*. Springer Verlag, Berlin
35. Coogan MP, Court JB, Gray VL, Hayes AJ, Lloyd SH, Millet CO, Pope SJA, Lloyd D (2010) Probing intracellular oxygen by quenched phosphorescent lifetimes of nanoparticles containing polyacrylamide-embedded  $[\text{Ru}(\text{dpp}(\text{SO}_3\text{Na})_2)_3]\text{Cl}_2$ . *Photochem Photobiol Sci* 9(1):103–109
36. Murphy MP (2009) How mitochondria produce reactive oxygen species. *Biochem J* 417: 1–13
37. Mik EG, Ince C, Eerbeek O, Heinen A, Stap J, Hooibrink B, Schumacher CA, Balestra GM, Johannes T, Beck JF, Nieuwenhuis ABF, vanHorsen P, Spaan JA, Zuurbier CJ (2009) Mitochondrial oxygen tension within the heart. *J Mol Cell Cardiol* 46:943–951
38. Wilhelm E, Battino OR, Woodcock RJ (1977) Low pressure solubility of gases in liquid water. *Chem Rev* 77:219–250
39. Wittenberg BA, Wittenberg JB (1989) Transport of oxygen in muscle. *Ann Rev Physiol* 51:857–878
40. Chance B, Noka S, Warren W, Yurtsever G (2005) Mitochondrial NADH as the bell-wether of tissue  $\text{O}_2$  delivery. *Adv Exp Biol Med* 566:231–262
41. Lloyd D, Mellor H, Williams JL (1983) Oxygen affinity of the respiratory chain of *Acanthamoeba castellanii*. *Biochem J* 17:143–146
42. Aon MA, Cortassa S, Marban S, O'Rourke B (2005) Synchronized whole cell oscillations in mitochondrial metabolism triggered by local release of reactive oxygen species in cardiac myocytes. *J Biol Chem* 278:44735–44744
43. Lemar KL, Aon MA, Cortassa S, O'Rourke B, Müller CT, Lloyd D (2007) Diallyl disulphide depletes glutathione in *Candida albicans* oxidative stress-mediated cell death studied by two-photon microscopy. *Yeast* 24:695–706
44. Aon MA, Cortassa S, O'Rourke B (2010) Redox-optimized ROS balance: a unifying hypothesis. *Biochim Biophys Acta* 1797(6–7):865–877
45. Jones DP, Mason HS (1978) Gradients of  $\text{O}_2$  in hepatocytes. *J Biol Chem* 253:4874–4880
46. Vanderkooi M, Wright WW, Erecinska M (1990) Oxygen gradients in mitochondria examined with delayed luminescence from excited-state triplet probes. *Biochemistry* 29:5332–5338
47. Vinogradov SA, Lo LW, Jenkins WT, Evans SM, Koch C, Wilson DF (1996) Noninvasive imaging of the distribution in oxygen in tissue *in vivo* using near-infrared phosphors. *Biophys J* 70:1609–1617
48. Mik EG, Johannes T, Zuurbier C, Jeinen A, Houben-Weerts JH, Balestra GM, Stap J, Beck JF, Ince C (2008) *In vivo* mitochondrial oxygen tension measured by a delayed fluorescence lifetime technique. *Biophys J* 95:3977–3990
49. Carraway ER, Demas JN, Degraff BA, Bacon JR (1991) Photophysics and photochemistry of oxygen sensors based on luminescent transition metal complexes. *Anal Chem* 63:337–342
50. Mik EG, van Leeuwen TG, Raat NJ, Ince C (2004) Quantitative determination of localised oxygen concentration *in vivo* by two-photon excitation phosphorescence lifetime measurements. *J Appl Physiol* 97:1962–1969
51. Vaughan WM, Weber G (1970) Oxygen quenching of pyrenebutyric acid fluorescence in water. A dynamic probe of the environment. *Biochemistry* 9:464–473
52. Knopp JA, Longmuir IS (1972) Intracellular measurement of oxygen by quenching of fluorescence of pyrenebutyric acid. *Biochim Biophys Acta* 279:393–397
53. Benson DH, Knopp JA, Longmuir IS (1980) Intracellular oxygen measurements of mouse liver cells using quantitative fluorescence video microscopy. *Biochim Biophys Acta* 591: 187–197
54. Mulazzani QG, Sun H, Hoffman MZ, Ford WE, Rodgers MAJ (1994) Quenching of the excited states of ruthenium (II)-diimine complexes by oxygen. *J Phys Chem* 98:1145–1150

55. Gafney HD, Adamson AW (1972) Excited state Ru(bipy)<sub>3</sub><sup>2+</sup> as an electron-transfer reductant. *J Am Chem Soc* 94:8238
56. Watts RJ, Crosby GA (1971) Spectroscopic characterization of complexes of ruthenium (II) and iridium (II) with 4, 4'-diphenyl 2, 2'-bipyridine and 4,7-diphenyl-1,10-phenanthroline. *J Am Chem Soc* 93:3184–3188
57. Winterle JS, Kliger DS, Hammond GS (1976) Mechanisms of photochemical reactions in solution. *J Am Chem Soc* 98:3719
58. Orellana G, Garcia-Fresnadillo D (2004) Optical sensors: industrial, environmental and diagnostic applications, vol 1. Springer, Berlin and Heidelberg, pp 309–357
59. Zahir KO, Haim AJ (1992) Yields of singlet dioxygen produced by the reaction between the excited state of trio (bipyridine) ruthenium (II) and triplet dioxygen in various solvents. *J Photochem Photobiol A Chem* 63:167–172
60. Tan-Sien-Hec L, Jacquet L, Kirsch-deMesmacker A (1994) Quenching of excited polyazaaromatic Ru(II) complexes by oxygen: evidence for an electron transfer process by photo electrochemical study. *J Photochem Photobiol A Chem* 8:169–176
61. Bacon JR, Demas JN (1987) Determination of oxygen concentrations by luminescence quenching of a polymer-immobilized transition-metal complex. *Anal Chem* 59:2780–2785
62. Garcia-Fresnadillo D, Georgiadou Y, Oranella G, Braun AM, Oliveros E (1996) Singlet-Oxygen (<sup>1</sup>Δ<sub>g</sub>) production by ruthenium complexes containing poly aza heterocyclic ligands in methanol and in water. *Helvet Chim Acta* 79:1222–1238
63. Kuimova MK, Yahioglu G, Ogilby PR (2009) Singlet oxygen in a cell: spatially depended lifetimes and quenching rate constants. *J Am Chem Soc* 131:332–340
64. Breitenbach T, Kuimova MK, Gbur P, Hatz S, Schack NB, Pedersen BW, Lambert JDC, Poulsen L, Ogilby PR (2009) Photosensitized production of singlet oxygen: spatially-resolved optical studies in single cells. *Photochem Photobiol Sci* 8:442–452
65. Hatz S, Poulsen L, Ogilby PR (2008) Time-resolved singlet oxygen phosphoresences measurements from photosensitized experiments in single cells: effects of oxygen diffusion and oxygen concentration. *Photochem Photobiol* 84:1284–1290
66. Finikova OS, Lebedev AY, Aprelev A, Troxler T, Gao F, Garnacho C, Muro S, Hochstrasser RM, Vinogradov SA (2008) Oxygen microscopy by two-photon-excited phosphorescence. *Chem Phys Chem* 9:1673–1679
67. Yaseen MA, Srinivasan VJ, Sakadžić S, Wu W, Ruvinskaya S, Vinogradov SA, Boas DA (2009) Optical monitoring of oxygen tension in cortical microvessels with confocal microscopy. *Opt Express* 17:22341–22350
68. Payra P, Dutta PK (2003) Development of a dissolved oxygen sensor using tris(bipyridyl) ruthenium (II) complexes entrapped in highly siliceous zeolites. *Microporous Mesoporous Mater* 64:109–118
69. Clark HA, Hoyer M, Parus S, Philbert MA, Kopelman R (1999) Optochemical nanosensors and subcellular applications in living cells. *Mikrochim Acta* 131:121–128
70. Buck SM, Koo Y-EL, Park E, Xu H, Philbert MA, Brasuel MA, Kopelman R (2004) Optochemical nanosensor PEBBLES: photonic explorers for bioanalysis with biologically localized embedding. *Curr Opin Chem Biol* 8:540–546
71. Poulsen AK, Arleth L, Almdal K, Scharff-Poulsen AM (2007) Unusually large acrylamide induced effect on the droplet size in AOT/Brij30 water-in-oil microemulsions. *J Colloid Interf Sci* 306:143–153
72. Poulsen AK, Scharff-Poulsen AM, Olsen LF (2007) Horseradish peroxidase embedded in polyacrylamide nanoparticles enables optical detection of reactive oxygen species. *Anal Biochem* 366:29–36
73. Castellano FN, Lakowicz JR (1998) A water-soluble luminescence oxygen sensor. *Photochem Photobiol* 67:179–183
74. Sud D, Zhong W, Beer DG, Mycek M-A (2006) Time-resolved optical imaging provides a molecular snapshot of altered metabolic function in living human cancer cell models. *Opt Express* 14:4412–4426

75. Sud D, Mycek M-A (2009) Calibration and validation of an optical sensor for intracellular measurements. *J Biol Optics* 14(2):020506
76. Bradley M, Alexander L, Duncan K, Chennaoui M, Jones AC, Sanchez-Martin RM (2008) pH sensing in living cells using fluorescent microspheres. *Bioorg Med Chem Lett* 18:313–317
77. Owen DM, Lanigan PM, Dunsby C, Munro I, Grant D, Neil MAA, French PMW, Magee AI (2006) Fluorescence lifetime imaging provides enhanced contrast when imaging the phase sensitive dye di-4-ANNEPPDHQ in model membranes and living cells. *Biophys J* 90:L80–82
78. Levitt JA, Matthews DR, Ameer-Beg SM, Suhling K (2009) Fluorescence lifetime and polarization-resolved imaging in cell biology. *Curr Opin Biotechnol* 20:28–36
79. Manjon F, Garcia-Fresnadillo D, Orellana G (2009) Water disinfection with Ru (ii) photosensitisers supported on ionic porous silicones. *Photochem Photobiol Sci* 8:926–932
80. Ramshesh VK, Lemasters JJ (2008) Pinhole shifting lifetime imaging microscopy. *J Biomed Opt* 13(6):064001
81. Parker D, Williams JAG (1996) Getting excited about lanthanide complexation chemistry. *J Chem Soc Dalton Trans* 3613–3628
82. Gawryszewska P, Sokolnicki J, Legendziewicz J (2005) Photophysics and structure of selected lanthanide compounds. *Coord Chem Rev* 249:2489–2509
83. Beeby A, Clarkson IM, Dickins RS, Faulkner S, Parker D, Royle L, de Sousa AS, Williams JAG, Woods M (1999) Non-radiative deactivation of the excited states of europium, terbium and ytterbium complexes by proximate energy-matched OH, NH and CH oscillators: an improved luminescence method for establishing solution hydration states. *J Chem Soc Perkin Trans* 2:493
84. Pope SJA (2007) Dual-emissive complexes: visible and near-infrared luminescence from bis-pyrenyl lanthanide(III) complexes. *Polyhedron* 26:4818
85. Andrews M, Laye RH, Harding LP, Pope SJA (2008) Quinoxaline sensitised lanthanide ion luminescence: syntheses, spectroscopy and X-ray crystal structure of Na{1,4,7-tris[(N-diethyl) carbamoylmethyl]-1,4,7,10-tetraazacyclododecane-10-(2-methylquinoxaline)}I-3 C<sub>7</sub>H<sub>8</sub>. *Polyhedron* 27:2365
86. Andrews M, Ward BD, Laye RH, Kariuki BM, Pope SJA (2009) Sensitized lanthanide-ion luminescence with aryl-substituted N-(2-nitrophenyl)acetamide-derived chromophores. *Helvet Chim Acta* 92:2159
87. Edward R (2009) Use of DNA-specific anthraquinone dyes to directly reveal cytoplasmic and nuclear boundaries in live and fixed cells. *Mol Cells* 27:391–396
88. Paul G, Palumbo M, Antonello C, Meloni GA, Marciani-Magno S (1986) A search for potential antitumor agents: biological effects and DNA binding of a series of anthraquinone derivatives. *Mol Pharmacol* 29:211–217
89. He ZE, He MF, Ma SC, But PPH (2009) Anti-angiogenic effects of rhubarb and its anthraquinone derivatives. *J Ethnopharmacol* 121:313–317
90. Pickhardt M, Gazova Z, von Bergen M, Khlistunova I, Wang YP, Hascher A, Mandelkow EM, Biernat J, Mandelkow E (2005) Anthroquinones inhibit tau aggregation and dissolve Alzheimer's paired helical filaments in vitro and in cells. *J Biol Chem* 280:3628–3635
91. Jones JE, Pope SJA (2009) Sensitized near-IR lanthanide luminescence exploiting anthraquinone-derived chromophores: syntheses and spectroscopic properties. *Dalton Trans* 39:8421–8425
92. dos Santos CMG, Harte AJ, Quinn SJ, Gunnlaugsson T (2008) Recent developments in the field of supramolecular lanthanide luminescent sensors and self-assemblies. *Coord Chem Rev* 252:2512
93. Que EL, Domaille DW, Chang CJ (2008) Metals in neurobiology: probing their chemistry and biology with molecular imaging. *Chem Rev* 108:1517–1549
94. Pope SJA, Laye RH (2006) Design, synthesis and photophysical studies of an emissive, europium based, sensor for zinc. *Dalton Trans* 25:3108–3113
95. Andrews M, Amoroso AJ, Harding LP, Pope SJA (2010) Responsive, di-metallic lanthanide complexes of a piperazine-bridged bis-macrocyclic ligand: modulation of visible luminescence and proton relaxivity. *Dalton Trans* 39:3407–3411
96. Coldwell JB, Felton CE, Harding LP, Moon R, Pope SJA, Rice CR (2006) Barium induced modulation of NIR emission in a neodymium cryptate complex. *Chem Commun* 5048–5050

Reviews in Fluorescence 2010

Geddes, C.D. (Ed.)

2012, XII, 380 p.,

ISBN: 978-1-4419-9828-6